DIRECT PROCEDURE TO CHARACTERIZE THE TENSILE CONSTITUTIVE BEHAVIOR OF STRAIN-SOFTENING AND STRAIN-HARDENING UHPFRC

Eduardo J. Mezquida-Alcaraz,[a,*] Juan Navarro-Gregori,[a] Pedro Serna-Ros.[a]

[a] Instituto de Ciencia y Tecnología del Hormigón (ICITECH), Universitat Politècnica de València, Camino de Vera s/n, 46022, Valencia, Spain.

[*] Tel.: +34 636 621 938

E-mail address: edmezal@alumni.upv.es

ABSTRACT

There is a need to establish a complete process to characterize Ultra-High-Performance Fiber-Reinforced Concrete (UHPFRC) in both strain-hardening and strain-softening tensile behavior. This process should be simple and easy to apply so that its application is direct. Therefore, this paper presents the development of a complete process to obtain the tensile constitutive parameters of UHPFRC. A simplified inverse analysis based on four-point bending tests (4PBT) to derive the tensile material properties of strain-hardening UHPFRC was adapted to be applied in the event of strain softening using a nonlinear finite element model (NLFEM). To fulfill this objective, an extensive experimental program was run with 227 UHPFRC specimens tested in 4PBT that exhibited strain-softening and strain-hardening tensile responses. As a reference, the characteristic UHPFRC tensile constitutive behavior was obtained. Finally, a predictive application capable of predicting tensile behavior using the experimental 4PBT curve as input was developed with the experimental database.

Keywords: strain-softening behavior, ultra-high performance fiber-reinforced concrete, finite element model, numerical validation, experimental four-point bending tests, prediction.

1. Introduction and objectives

Ultra-High-Performance Fiber-Reinforced Concrete (UHPFRC) is a concrete capable of reaching very high compressive strength: 120-200 MPa. Normally, this concrete type is reinforced with fine steel fibers to confer ductility and high tensile strength: 7-12MPa. This special bearing capacity is a direct consequence of its dense microstructure, which also provides an impervious matrix with no capillarity pores to prevent aggressive substances (liquids and gases) from penetrating because they can generate corrosion [1,2]. Compared to conventional and high-strength concretes, UHPFRC can generate forms of construction that save materials, which means that it is especially sustainable [3,4].

UHPFRC can be considered a special type of high-performance fiber-reinforced cement composite (HPFRCC) if the definition in the Preface in the 6th and 7th Symposia on HPFRCC [5,6] and JSCE recommendations [7] is used. It states that all those concretes exhibiting a strain-hardening tensile stress-strain response accompanied by multiple cracking and a relatively high energy absorption capacity can be considered HPFRCC. Reaching strain-hardening behavior in a UHPFRC matrix depends on fiber type and content, matrix strength, the bond between matrix and fibers, and on specimen size and geometry, pouring system, support conditions, structural redundancy, etc.

Currently, the characterization of UHPFRC tensile behavior can be assumed a challenge. Mainly, UHPFRC tensile properties are determined using uniaxial tensile tests and bending tests. Even though in tensile tests the tensile behavior is directly obtained, their experimental setup is complicated and requires specific preparation for alignment and gripping the specimen that frequently leads to inaccurate results [8,9]. On the other hand, notched three-point bending tests are considered not suitable for strain-hardening materials as they lead to an overestimation of tensile properties as a consequence of their multi-microcracking phase [10]. Therefore, due to their simplicity, four-point bending tests (4PBT) are one of the best tests to achieve this purpose. Nevertheless, they require running an inverse analysis methodology to derive tensile properties based on the obtained results. In line with this, different inverse analysis methods

have been developed to obtain the parameters that constitute UHPFRC tensile behavior from 4PBT [11–21]. Two kinds are mainly considered: simplified methods defined from the key points extracted from experimental 4PBT; methods defined from the complete experimental curve. The latter can also be divided into iterative and point-by-point methods. In point-by-point inverse methods, the shape of the UHPFRC tensile stress-strain relation is not necessarily assumed [15,17]. With iterative ones, a constitutive behavior has to be previously defined to apply the analytical or numerical process to obtain a response that can be compared to the experimental response and to, consequently, start the iterative process. Several analytical methods based on closed-form formulations and numerical methods based, in turn, on nonlinear 2D-FEM using fracture mechanics to obtain the theoretical curve in load-deflection, load-strain or load-curvature terms can be found in [13,14,19,21]. These methods are based on the complete experimental curve and are indicated for computer analyses. As these methods are normally accurate, they are employed in the research field. Simplified methods resort to a few specific points from the results obtained with 4PBT [13,22–25]. The idea of developing these simplified methods lies in their direct application to structural design or quality control so they are "easy to conduct". Even though these methods seem easy to apply, they are not completely accurate and objective, and are subjected to variations depending on the type of application.

At this point it is important to introduce how standards and design rules consider tensile constitutive behavior. Australia follows the recommendations of Ductal® properties [26] which, for tensile constitutive behavior, propose using experimental direct tensile tests as a source, namely trilinear stress-strain behavior in which the two first lines represent perfect elastoplastic behavior and the third is the softening branch until zero stress. The yielding tensile stress is considered at 5MPa with an elastic strain of 0.0001. The ultimate tensile strain at the end of the plastic branch is considered at $\varepsilon_{t,p} = 0.16\, L_f / 1.2D \leq 0.004$, where L_f is the length of fibers, D the overall beam depth and, finally, the strain at zero stress is considered $\varepsilon_{t,u} = L_f / 1.2D \leq 0.01$. In the Japan Society of Civil Engineering considerations [27], a tensile test is performed. As a result, the tensile curve is defined by the tensile yield strength and the ultimate tensile strength and strain. The Japan recommendations consider only strain-hardening tensile behavior. For calculations however, they propose a perfect elastoplastic model. When the design-cross-sectional strength is underestimated in an analysis, the tensile stress-strain relation should be appropriately reevaluated, and the failure mode also needs to be confirmed with a model that appropriately reflects the stress-strain relation of HPFRCC. In the USA, the FHWA (Federal Highway Administration) [28] refers to the UHPC idealized response with strain-hardening behavior in tension obtained from direct tensile tests. Graybeal has reported tensile strength measurements using flexural prisms (by considering inverse analyses to obtain their tensile constitutive response), split cylinders, mortar briquettes and direct tension tests of cylinders depending on the heat treatment. Adaptation of standards for conventional concrete has been made to make it appropriate to quantitatively assess the post-cracking tensile response of UHPC. However, this seems appropriate for setting the response in the direction of strain-hardening UHPFRC tensile behavior. The French standard for UHPFRC [29,30], which is based on recommendations [23], proposes classifying UHPFRC tensile behavior into three classes: T1 ("*strain-softening fiber-reinforced concrete*"): those UHPFRC in which both the average and characteristic f_{tu} (ultimate tensile strength) values are lower than f_t (yielding tensile stress); T2 ("*low strain-hardening fiber-reinforced concrete*"): those in which the characteristic f_{tu} value is lower than f_t, but is not the average value; T3 ("*high strain-hardening concrete*"): those in which both the average and characteristic f_{tu} values are higher than f_t. Depending on the UHPFRC class, a different tensile constitutive law can be used. For classes T1 and T2, the parameters required to determine tensile law derive from notched three-point bending tests and the associated inverse analysis procedure; for class T3, an unnotched 4PBT and the associated inverse analysis are needed. Regardless of class type, the French standard applies two different tests: one to determine cracking strength and another to determine other tensile parameters. Moreover, the specimen geometry for the characterization test depends on fiber length and structural size. The Swiss standard [22] considers the following to be indicative values of UHPFRC tensile parameters: f_t =7-12 MPa, f_{tu} = 7-15 MPa and ε_{tu} = 0-3.5‰ (strain at ultimate tensile strength). To define tensile behavior, two experimental tests can be used: direct tensile tests to obtain the force-displacement experimental curve; a 4PBT and a simplified inverse analysis to derive the tensile response from the experimental load-deflection on the mid-span curve from 4PBT. The Swiss standard classifies UHPFRC into types U0, UA and UB according to tensile parameters: $f_{t,k}$, $f_{tu,k}/f_{t,k}$ and ε_{tuk}, that is: $f_{t,k} \geq 7$ MPa for U0 and UA and $f_{t,k} \geq 8.5$ for UB, $f_{tu,k}/f_{t,k} > 0.7$ for U0, $f_{tu,k}/f_{t,k} > 1.1$ for UA and $f_{tu,k}/f_{t,k} > 1.2$ for UB, ε_{tuk} *(‰)*$= f_t/E$ for U0 ε_{tuk} *(‰)*> 1.5 for UA and ε_{tuk} *(‰)*> 2 for UB.

The French [23] and Swiss [22] standards, which can be considered two of the most referenced standards for UHPFRC in Europe, contemplate both strain-hardening (SH) and strain-softening (SS) UHPFRC. Therefore, the authors of this work noticed a need to establish a complete process to characterize UHPFRC tensile behavior in either SH or SS. This application of this process should be simple and easy. Consequently, this paper presents the development of a complete process to obtain the tensile constitutive parameters of UHPFRC that is simple and direct. The considered experimental test is 4PBT. To obtain tensile constitutive behavior, a simplified inverse analysis (4P-IA), developed by our group in previous works [24,25], was carried out from the experimental stress-deflection on the mid-span curve. To determine the validity and accuracy of this inverse analysis method, a nonlinear finite element model (NLFEM) presented in [31,32] was developed. As this 4P-IA was developed for UHPFRC, which exhibits SH behavior, NLFEM was used to adapt and calibrate the inverse analysis for UHPFRC, which exhibits SS tensile behavior.

This paper is organized as follows: Section 1 is an introduction to explain the purposes of this paper. Section 2 briefly presents the experimental 4PBT, the simplified inverse analysis (4P-IA) and NLFEM. Section 3 offers a UHPFRC 4PBT experimental program to generate a database to apply 4P-IA and NLFEM in SH and SS cases. Section 4 describes the NLFEM validation to adapt and calibrate 4P-IA in SS cases. This section also established a correction of 4P-IA to be applied in SS UHPFRC cases. Section 5 explains the obtained reference for characteristic UHPFRC tensile behavior. Section 6 proposes an application to integrate the whole process to predict the constitutive tensile parameters from the experimental 4PBT stress-deflection at the mid-span curve. Finally, Section 7 indicates the most relevant conclusions drawn from this work.

2. The process: Experimental Test, 4P-IA and NLFEM

To obtain the tensile behavior of UHPFRC, the unnotched 4PBT was considered by the authors to be the most suitable test because it provides a large area with a relatively constant bending moment. Therefore, the micro-cracking process that characterizes this concrete in its hardening part was free to develop (see Figure 1). In this case, specimens of 100x100x500mm were used in order to analyze the consequences of applying the same methodology to the case of UHPFRC that exhibits strain-softening constitutive tensile behavior. The experimental test and setup are fully described in [10,24].

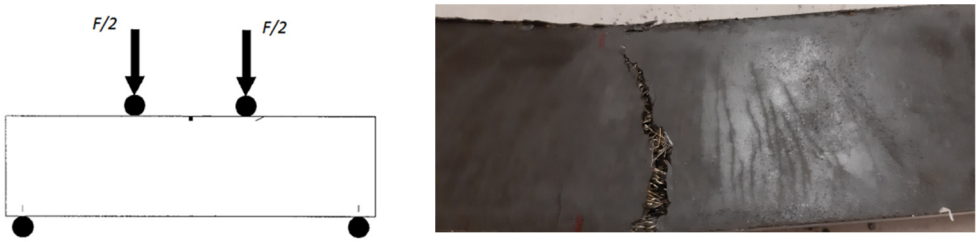

Figure 1 Four-Point Bending Test and micro-cracking process of UHPFRC

As mentioned in the Introduction, the use of bending tests to obtain tensile behavior requires an inverse analysis. For this purpose, the authors chose an inverse analysis method that was developed properly in the research group for UHPFRC that exhibits SH behavior. The Simplified Four-Point Inverse Analysis Method (4P-IA), developed and explained in [10,24], is a simplified methodology based on the closed-form nonlinear hinge model developed in [10,25]. It entails having to select four specific key points extracted from the experimental 4PBT equivalent bending stress-displacement on the mid-span curve (Figure 2). Using these points, the parameters defining the assumed quadrilinear stress-strain law inside the hinge can be determined by a back-of-the-envelope calculation. This law is used to determine the constitutive tensile behavior of SH UHPFRC.

The proposed constitutive model for UHPFRC is depicted in Figure 2 according to six parameters: elastic modulus (E); cracking strength (f_t); ultimate cracking strength (f_{tu}) and its associated strain (ε_{tu}); crack opening at the intersection of the line that defines the initial slope to the w axis (w_0); the characteristic crack opening ($l_f/4$) defined as one fourth of fiber length.

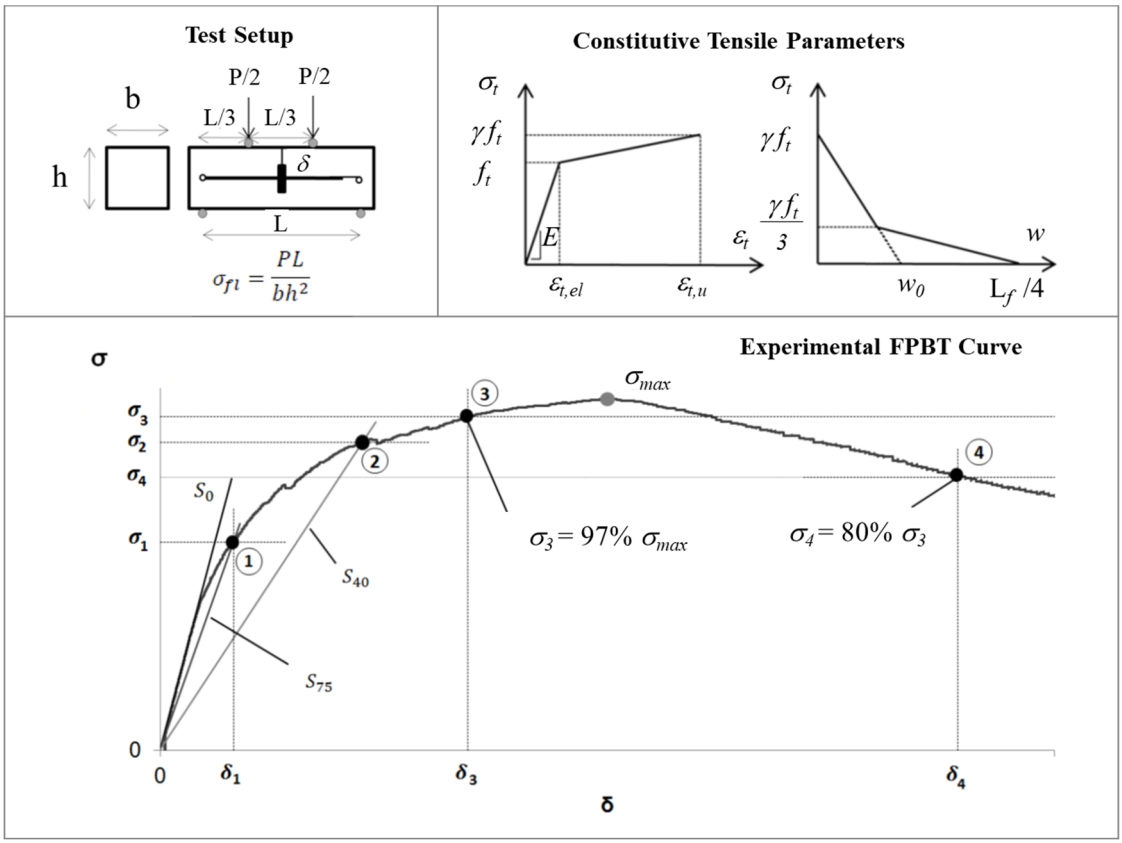

Figure 2 Simplified 4P-IA

If we bear all this in mind, we wonder what would happen if UHPFRC did not exhibit SH behavior? Would 4P-IA be reliable enough to obtain the tensile parameters of the UHFRC that exhibits SS behavior?

To distinguish between the UHPFRCs that exhibit SH behavior from those exhibiting SS behavior in tension, a hardening ratio (γ) was defined (1). If $\gamma \geq 1$, then UHPFRC would exhibit SH. If $\gamma < 1$, then UHPFRC would exhibit SS. Figure 3 illustrates this interpretation.

$$\gamma = \frac{f_{tu}}{f_t} \tag{1}$$

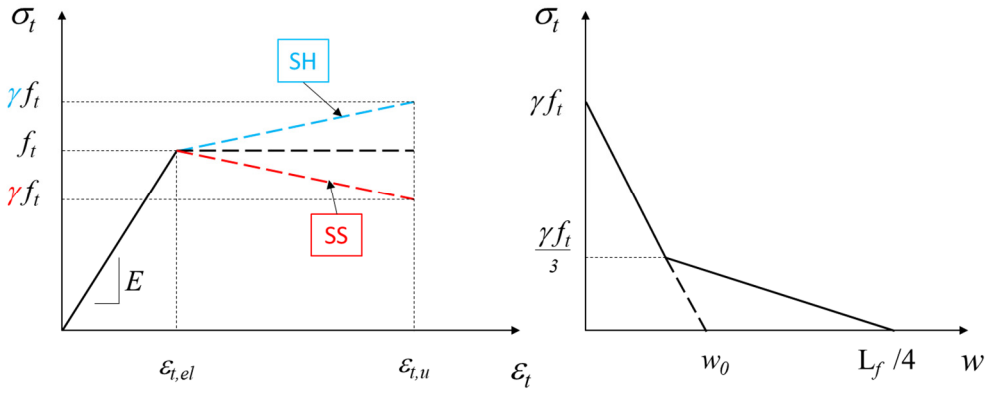

Figure 3. Constitutive behavior of UHPFRC with SH and SS

4P-IA was used for the UHPFRC exhibiting SH tensile constitutive behavior ($\gamma \geq 1$) [10]. In order to extend its application to the SS range ($\gamma < 1$), it was necessary to develop a nonlinear finite element model (NLFEM) to simulate 4PBT in order to test and calibrate the inverse analysis.

In this work, a numerical model developed by the authors in [31] to validate 4P-IA with SH UHPFRC using the FE software DIANA [33] was employed. A discrete cracking approach was followed to model tensile UHPFRC constitutive behavior. In this approach, the constitutive model for UHPFRC was based on the discrete cracking model as an interface behavior. The constitutive law for discrete cracking is based on a total deformation theory [33]. This behavior was forced only on the central beam section (Figure 4). To fulfill this objective, both tensile strength (f_t) and ultimate tensile strength (f_{tu}) were reduced by 2%. The rest of the beam was modeled by a smeared cracking approach based on a fixed total strain crack model expressed according to the crack opening curve.

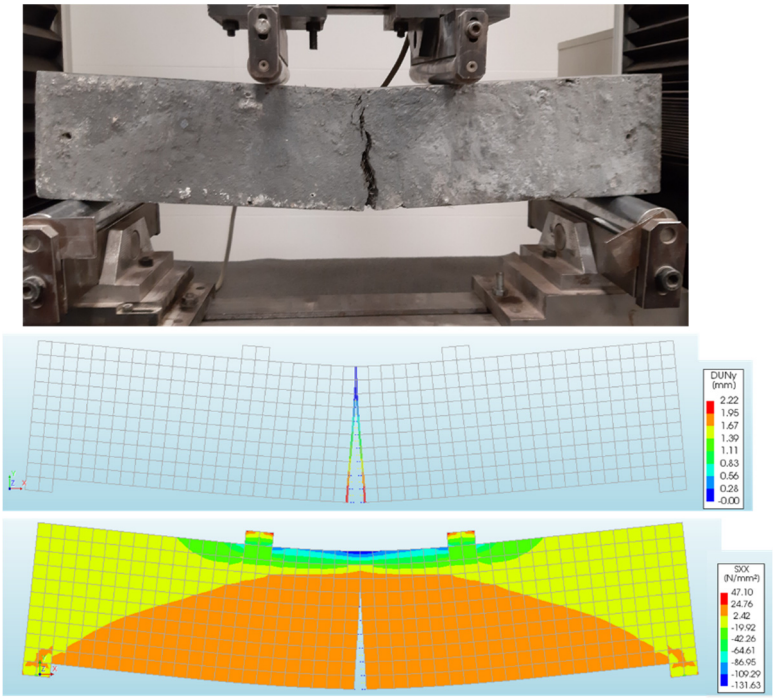

Figure 4. Discrete cracking approach.

4PBT were modeled with 2D quadratic plane stress eight-node quadrilateral elements. Quadratic 2D 3+3 nodes line interface elements were placed on the central beam section. The load was applied to the steel load plates by gradual increasing displacement. A nonlinear analysis was carried out by following an incremental-iterative solution procedure.

3. Experimental program

In order to generate a database of the tensile constitutive parameters obtained from 4P-IA, an experimental program of 227 UHPFRC specimens (100x100x500mm) was cast and tested in 4PBT (see Figure 5). Sixty-nine of them were cast using 1.53-1.66% (120-130 kg/m^3) in volumes of smooth-straight (13/0.20) steel fibers, and 158 with 2.00% (160 kg/m^3). According to Figure 5, two displacement transducers were used to record the displacement at the mid-span (δ) on the front and back sides. As a result, the load (P)-displacement at the mid-span (δ) curves was obtained. By using Expression (2), it was possible to represent the equivalent bending stress (σ)-displacement at the mid-span (δ) (see Figure 6).

$$\sigma = \frac{P \cdot L}{b \cdot h^2} \tag{2}$$

where, as seen in Figure 5, P is the load applied in 4PBT, L is the span between support rollers, b is specimen depth (100mm) and h is specimen height.

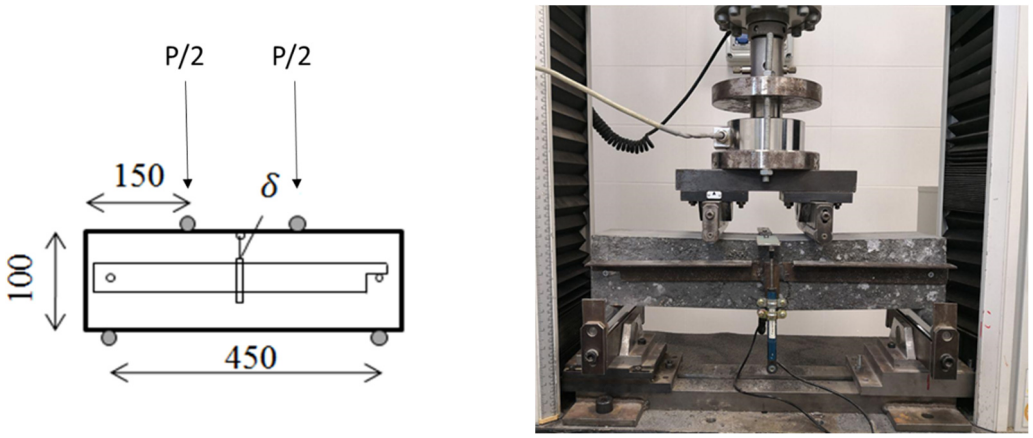

Figure 5. Four-Point Bending Test (4PBT)

Compressive strength was obtained from 100-mm cubes within a range of [99,172] MPa. The tensile parameters obtained from the 227 specimens fell within the following ranges:

$f_t \in [4.12\ ,\ 12.70]$ MPa

$f_{tu} \in [4.19\ ,\ 13.75]$ MPa

$\varepsilon_{tu} \in [0.96\ ,\ 8.75]$ ‰

$E \in [39100\ ,\ 56500]$ MPa

$w_0 \in [1.23\ ,\ 5.60]$ mm

$\gamma \in [0.51\ ,\ 1.68]$

Figure 6 depicts the experimental equivalent bending stress (σ)-displacement on the mid-span (δ) curves for the 158 specimens of 160 kg/m^3 and the 69 specimens of 120-130 kg/m^3 of fibers. The scatter observed in the results was considered acceptable based on the experience in previous research [10].

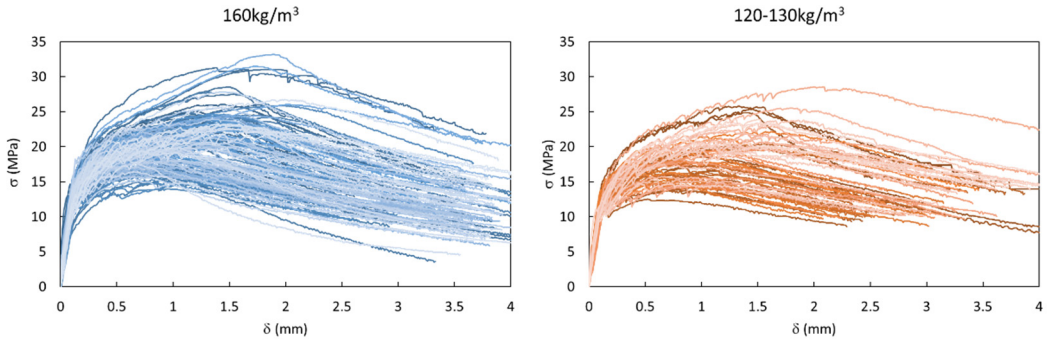

Figure 6. σ-δ curves for the specimens with 160 kg/m^3 (left) and 120-130 k/m^3 of fibers (right)

Using the σ-δ curves shown in Figure 6, 4P-IA was applied to each curve to obtain each specimen's tensile constitutive behavior. Figure 7 and Figure 8 depict the tensile constitutive behavior for the specimens with 160 kg/m^3 and 120-130 kg/m^3.

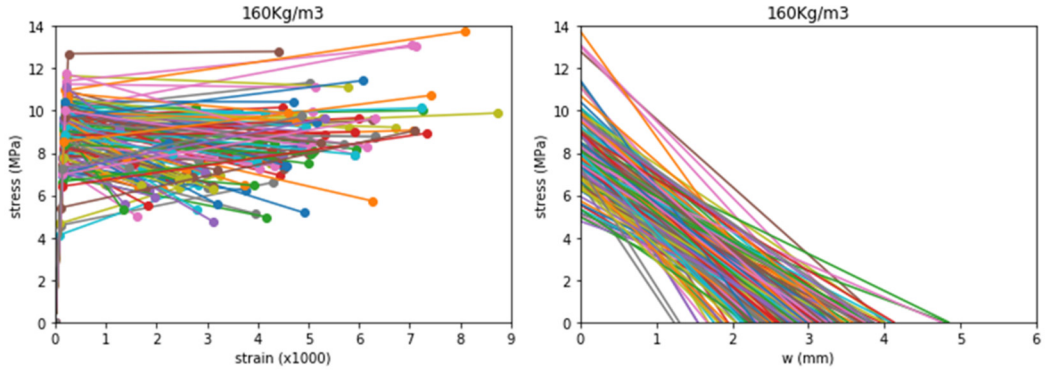

Figure 7 Constitutive behavior for the UHPFRC specimens with 160 kg/m³ of steel fibers

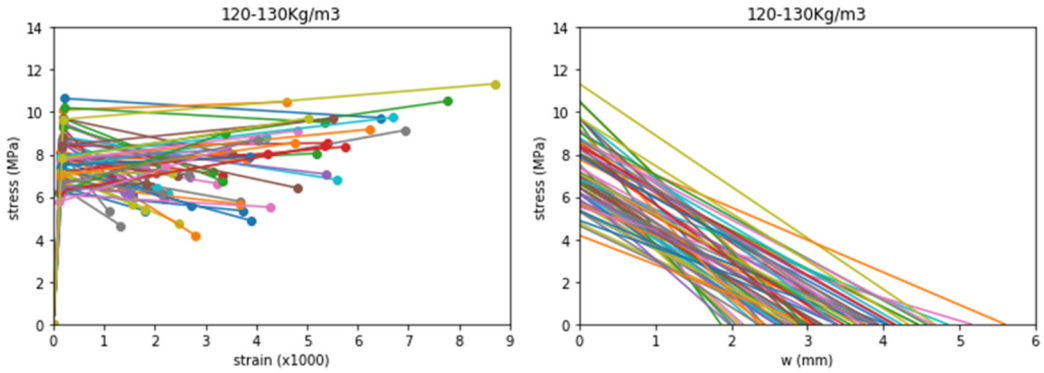

Figure 8 Constitutive behavior for the UHPFRC specimens with 120-130 kg/m³ of steel fibers

We may wonder about the need to use UHPFRC with SS. According to UHPFRC standards [22,23], it would seem that the concretes displaying SH behavior provide desirable behavior and guarantee good concrete. This may be right, but is sometimes questionable. In line with this, an analysis was done using the specimens from the experimental program. Figure 9 represents the P-δ curves for the specimens with similar f_t for both amounts of fibers: 160 kg and 130 kg. Table 1 shows the tensile constitutive parameters for these specimens. We observe that for an f_t value of around 9.5MPa for the 130 kg/m³ specimens and an f_t value of about 8.5MPa for 160 kg/m³, the P-δ response for the specimens that exhibited SH ($\gamma \geq 1$) accumulated more energy (in terms of area under the P-δ curve, Figure 9) than those exhibiting SS ($\gamma < 1$) with both amount of fibers. So in these cases, the SH response would appear to be more resistant than for the same f_t value.

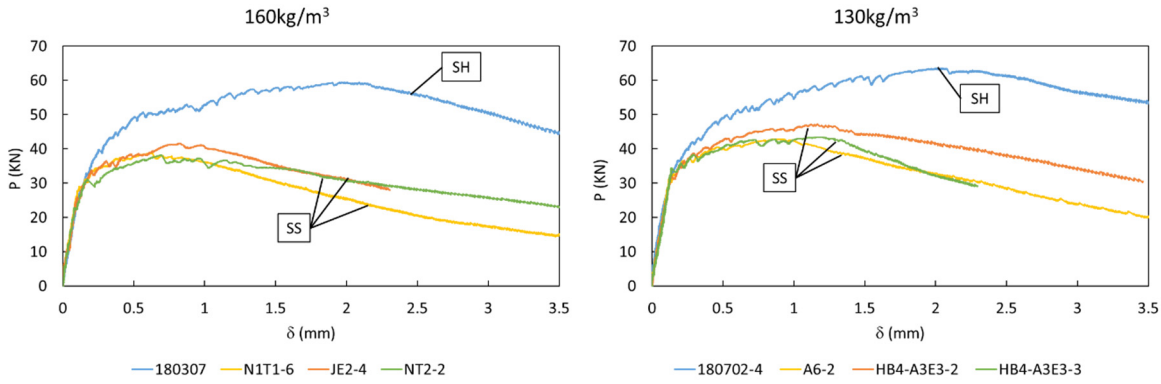

Figure 9 P-δ curves for the specimens with similar f_t values.

Table 1 Tensile constitutive parameters for the specimens with similar f_t values

130 kg/m3 of steel fibers						
Id.	f_t (MPa)	f_{tu} (MPa)	ε_{tu} (‰)	E (MPa)	w_o (mm)	γ
180702-4	9.66	11.34	8.71	50000	4.68	1.17
A6-2	9.50	6.93	2.68	50100	2.69	0.73
HB4-A3E3-2	9.70	8.01	3.52	49400	3.93	0.83
HB4-A3E3-3	9.42	7.48	2.20	50400	2.80	0.79
160 kg/m^3 of steel fibers						
Id.	f_t (MPa)	f_{tu} (MPa)	ε_{tu} (‰)	E (MPa)	w_o (mm)	γ
180307	8.54	10.73	7.42	50300	3.44	1.26
N1T1-6	8.47	6.66	1.65	50900	2.16	0.79
JE2-4	8.61	7.23	2.81	47800	2.48	0.84
NT2-2	8.25	6.34	2.46	53200	3.48	0.77

A comparison was made in energy terms. In Figure 10, the P-δ curves for the specimens with similar energy (similar area under the P-δ curve) are represented for both amounts of fibers: 160 kg and 130 kg. Table 2 shows the tensile constitutive parameters. In both cases (160 and 130), when the energy accumulated on the P-δ curve was similar for the specimens exhibiting SH and SS, the f_{tu} for the SH specimens came very close to the f_t for the SS specimens. A difference in stiffness appeared when the curve lost its linearity, which could explain SH/SS behavior. When comparing the specimens with SS to one another for both amounts of fibers, they showed different load levels at the loss of linearity point and at the maximum flexural load, which are represented in Figure 10 and, consequently, at the f_t and f_{tu} values (Table 2). They all had more or less the same stiffness up to loss of linearity. However, when comparing them to the specimen displaying SH behavior (Table 2), the change in stiffness became more evident (Figure 10).

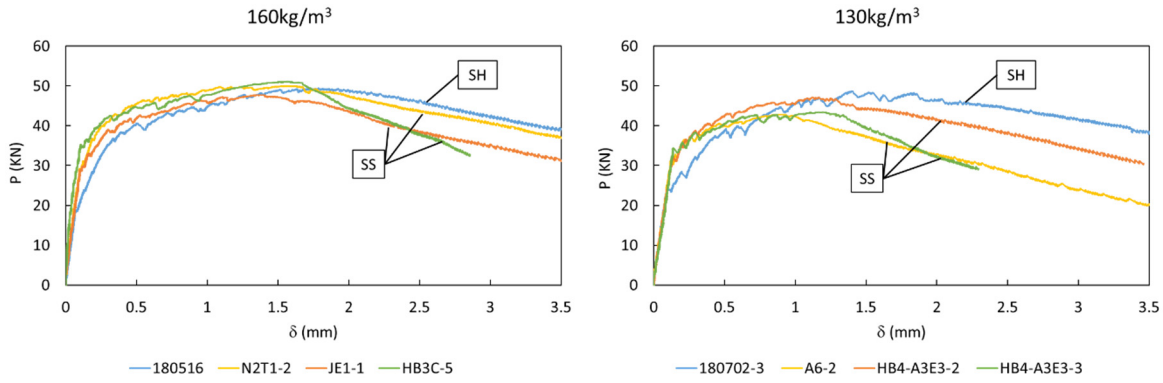

Figure 10. P-δ curves for the specimens with similar energy.

Table 2 Tensile constitutive parameters for the specimens with similar energy

130 kg/m^3 of Steel fibers						
Id.	f_t (MPa)	f_{tu} (MPa)	ε_{tu} (‰)	E (MPa)	w_o (mm)	γ
180702-3	6.17	9.15	6.93	52400	3.64	1.48
A6-2	9.50	6.93	2.68	50100	2.69	0.73
HB4-A3E3-2	9.70	8.01	3.52	49400	3.93	0.83
HB4-A3E3-3	9.42	7.48	2.20	50400	2.80	0.79
160 kg/m^3 of steel fibers						
Id.	f_t (MPa)	f_{tu} (MPa)	ε_{tu} (‰)	E (MPa)	w_o (mm)	γ
180516	5.41	9.06	7.11	56200	3.20	1.68
N2T1-2	9.42	8.49	4.32	53700	4.85	0.90
JE1-1	8.94	8.11	4.69	52100	3.70	0.91
HB3C-5	9.91	8.32	6.15	50200	3.16	0.84

It can be deduced for the UHPFRC specimens exhibiting SS behavior, versus those showing SH in Table 2 and Figure 10, that the concrete matrix could be more resistant for UHPFRC with SS and, therefore, the f_t value could be higher. The UHPFRC cases exhibiting SH behavior could be cast with a concrete matrix capable of reaching less strength and, consequently, the f_t parameter would lower. In this case, the steel fiber effect would make the f_{tu} value increase. This would mean that the concrete with SH would not necessarily be better than the concrete exhibiting SS. Consequently, if it were possible to ensure a high-resistant concrete matrix with the same amount of fibers, then concrete would display SS tensile behavior ($\gamma < 1$). However, the energy obtained in its P-δ experimental response came close to a concrete with SH tensile behavior ($\gamma \geq 1$), with an f_{tu} value of the SH concrete coming close to the f_t value of the SS concrete.

4. Numerical model application

The material constitutive parameters obtained from applying the simplified 4P-IA for 65 specimens from the experimental program were implemented into NLFEM (see Section 2) and compared to the experimental program results.

Figure 11 illustrates the comparison made between the experimental and numerical stress-deflection (σ-δ) curves for an SH specimen (Figure 11, left) and an SS specimen (Figure 11, right).

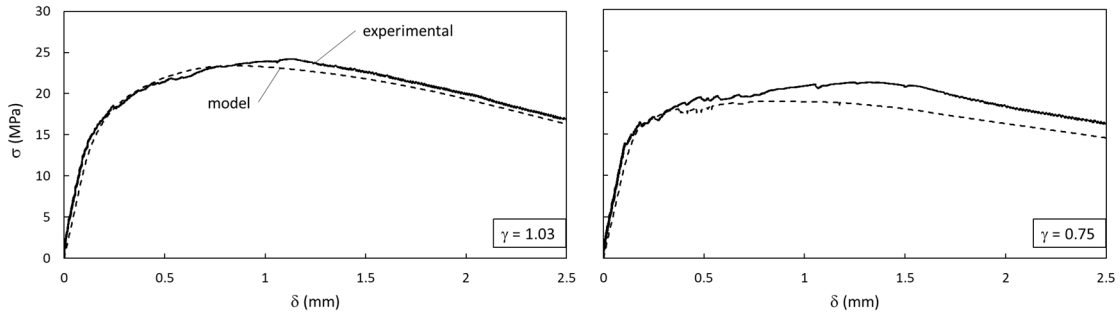

Figure 11. Specimen with SH (left); specimen with SS (right)

As seen in Figure 11, the σ-δ curve from NLFEM for the specimens displaying SH ($\gamma \geq 1$) was more accurate than for those exhibiting SS ($\gamma < 1$). Notwithstanding, the inaccuracy observed in the model's curve for the specimens showing SS was conservative.

To quantify the accuracy of the NLFEM response, a coefficient of accuracy (CS) was defined as the ratio between the experimental stress and the stress obtained from the model (3). This CS was obtained at four levels of the experimental deflection upon maximum experimental stress ($\delta_{\sigma maxexp}$): $0.25 \cdot \delta_{\sigma maxexp}$, $0.50 \cdot \delta_{\sigma maxexp}$, $\delta_{\sigma maxexp}$ and $1.25 \cdot \delta_{\sigma maxexp}$ (see Figure 12). The energy of the curve delimited by both the $\delta_{\sigma maxexp}$ (A1) and $1.25 \cdot \delta_{\sigma maxexp}$ levels (A2) for the experimental and model curves was obtained.

$$CS = \frac{\sigma_{exp}}{\sigma_{model}} \tag{3}$$

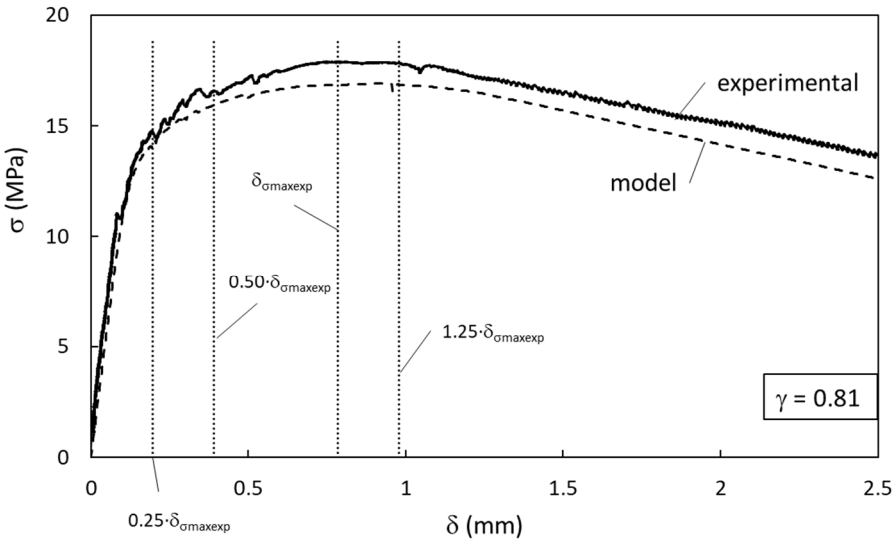

Figure 12. Coefficient of accuracy levels.

Figure 13 shows the relation between the hardening ratio (γ) and the CS at the four experimental deflection levels upon maximum experimental stress ($\delta_{\sigma maxexp}$): $0.25\cdot\delta_{\sigma maxexp}$, $0.50\cdot\delta_{\sigma maxexp}$, $\delta_{\sigma maxexp}$ and $1.25\cdot\delta_{\sigma maxexp}$ for the analyzed 65 specimens: 54 specimens of 160 kg/m^3 of fibers and 11 of 130 kg/m^3.

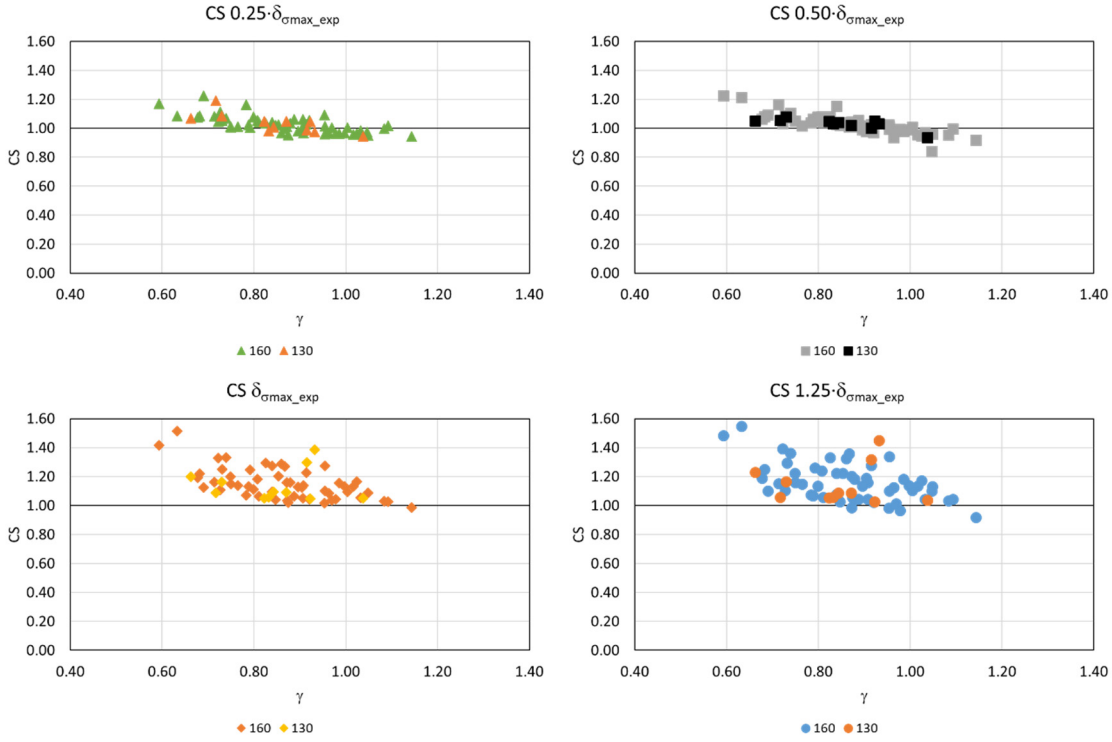

Figure 13. CS vs. γ at four δ levels

As observed in Figure 13, the CS came close to 1 in the early stages of the $\sigma-\delta$ curve (at $0.25\cdot\delta_{\sigma maxexp}$ and $0.50\cdot\delta_{\sigma maxexp}$), and clearly exceeded 1 at the $\delta_{\sigma maxexp}$ and $1.25\cdot\delta_{\sigma maxexp}$ levels. This meant that in the first stages, the model accurately predicted the experimental curve. When the highest level of the curve was reached and the descending branch took part, the model's accuracy was not as good as on the elastic branch, but was conservative. Therefore, the model was reliable enough. According to Figure 13, certain inaccuracy appeared at the first two levels, $0.25\cdot\delta_{\sigma maxexp}$ and $0.50\cdot\delta_{\sigma maxexp}$ (elastic branch of the $\sigma-\delta$ curve) on the non conservative side with the specimens made of UHPFRC exhibiting SH ($\gamma\geq 1$). Nevertheless, this inaccuracy

was negligible. At the last levels, and despite them being conservative, the stress experimental values were higher than the numerical ones, especially for SS ($\gamma < 1$). The model appeared more accurate in these stages for the UHPFRC specimens displaying SH behavior.

Figure 14 shows the relation between the energy calculated for the experimental ($A1_{exp}$) and numerical ($A1_{model}$) curves at the $\delta_{\sigma maxexp}$ level and the energy calculated for the experimental ($A2_{exp}$) and numerical ($A2_{model}$) curves at the $1.25 \cdot \delta_{\sigma maxexp}$ level for the same 65 specimens.

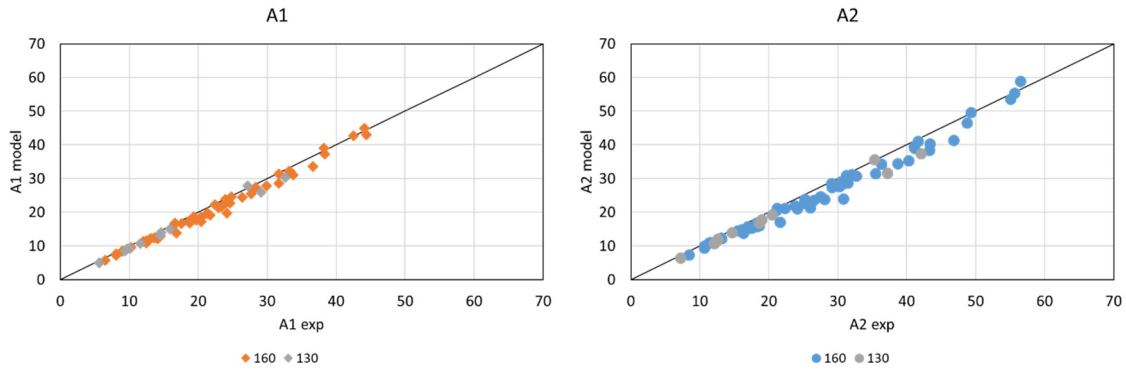

Figure 14. A1exp vs. A1model, A2exp vs. A2model.

As Figure 14 illustrates, the energy obtained in the experimental test was slightly higher than that obtained in the model. The same trend was observed for the other specimens in relation to the energy limited by $\delta_{\sigma maxexp}$ (A1) and $1.25 \cdot \delta_{\sigma maxexp}$ (A2). So the model was slightly conservative.

Figure 15 shows the relation between the experimental and numerical σ_{max} for the same 65 specimens.

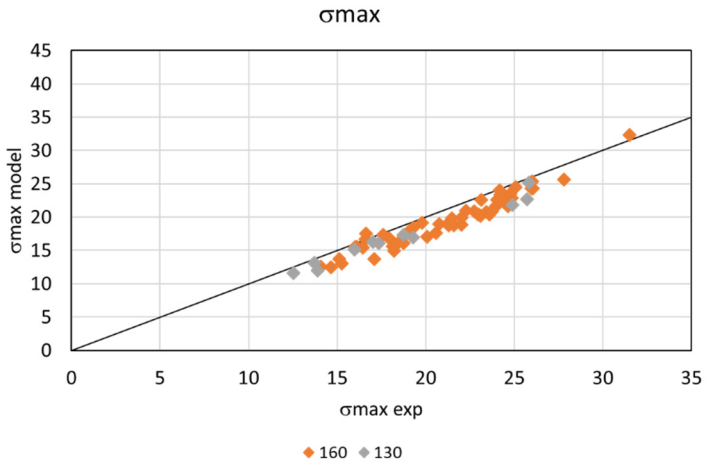

Figure 15. Experimental vs. model σ_{max}.

As shown in Figure 15, the experimental σ_{max} value was higher than the numerical one for each specimen. So as with energy, this value means that the model was conservative compared to the experimental results, and the level of accuracy was acceptable (see Figure 13, Figure 14 and Figure 15).

It is important to understand that the 4P-IA procedure was developed for UHPFRC manifesting SH behavior ($\gamma \geq 1$). The results in Figure 13, Figure 14 and Figure 15 demonstrate that the simplified inverse analysis method is applicable for SS, but can be considered too conservative. Therefore, a study of the adjustment of 4P-IA was run to obtain more accurate results and to reduce the conservative response in the UHPFRC exhibiting SS behavior ($\gamma < 1$). The idea was to adapt 4P-IA to cover all those cases that could appear when working with optimized UHPFRC; that is, SH behavior, but also SS.

The adjustment procedure consisted in calibrating the ε_{tu} and f_{tu} parameters to better fit the NLFEM σ-δ curve in 4PBT. A parametrical study focussing on the ε_{tu} and f_{tu} parameters was done to study their influence on the σ-δ response. By way of example, Figure 16 shows the experimental σ-δ at the mid-span of an SS specimen with 130 kg/m^3. If 4P-IA was applied and the resulting tensile parameters were used in NLFEM, the obtained σ-δ response would be conservative, as seen in Figure 16 (left). Therefore, f_{tu} was incremented by a percentage to study its influence on the σ-δ response. As shown in Figure 16 (right), the σ-δ response very accurately adjusted the experimental one when f_{tu} was incremented by 7% of the original value. Table 3 shows the tensile constitutive parameters after applying 4P-IA, which were used in NLFEM (see Figure 16, left) and the same parameters with the 7% f_{tu} increment employed in NLFEM (see Figure 16, right).

Therefore, the f_{tu} parameter directly influenced the model's response and, as we can see, 4P-IA underestimated the f_{tu} value, which gave a conservative result in the σ-δ response and, consequently, in the energy that took part in the flexural response of UHPFRC with SS behavior.

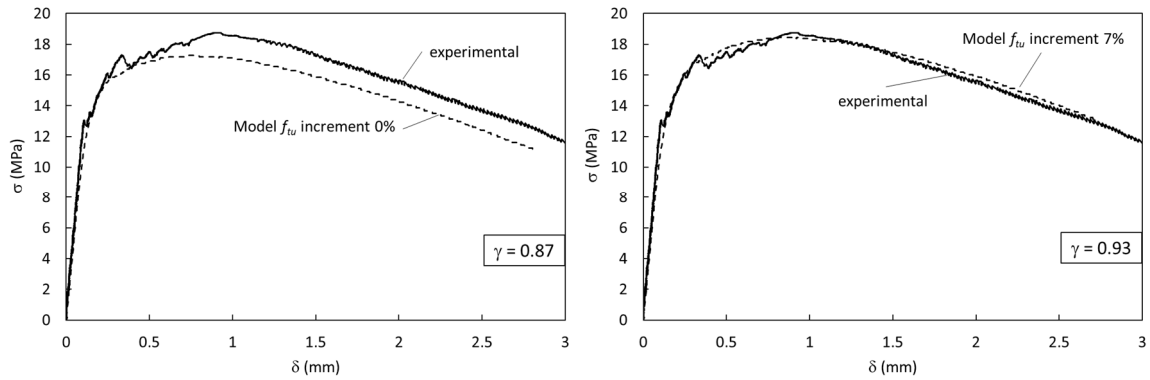

Figure 16. σ-δ response of the f_{tu} variation in a strain-softening behavior specimen.

Table 3. Constitutive tensile parameters from applying 4P-IA and f_{tu} variation

	constitutive tensile law					
	f_t (MPa)	f_{tu} (MPa)	ε_{tu} (‰)	E (MPa)	w_o (mm)	γ
4P-IA	8.08	7.03	3.35	54400	3.11	0.87
f_{tu} 7% inc.	8.08	7.52	3.35	54400	3.11	0.93

The parametric study then focused on the ε_{tu} parameter. By way of example, the experimental σ-δ on the mid-span curve for the same specimen as in Figure 16 is depicted in Figure 17. In this case, the f_{tu} value remained because the value obtained from the simplified 4P-IA and the parameter that varied was ε_{tu}. Figure 17 (left) shows the σ-δ response of NLFEM when ε_{tu} was incremented by 100% of the ε_{tu} value obtained with 4P-IA. In Figure 17 (right), the σ-δ curve from NLFEM when ε_{tu} was incremented by 200% is found. Table 4 shows the tensile constitutive parameters after applying the simplified 4P-IA, which were the same parameters with the 100% ε_{tu} increment and the same parameters with the 200% ε_{tu} increment employed in NLFEM in Figure 17. Therefore, as shown in Figure 17 and Table 4, the variation in the ε_{tu} parameter needed to be very wide to have some effect on the model's σ-δ response. Consequently, the influence of the variation in ε_{tu} was considered negligible.

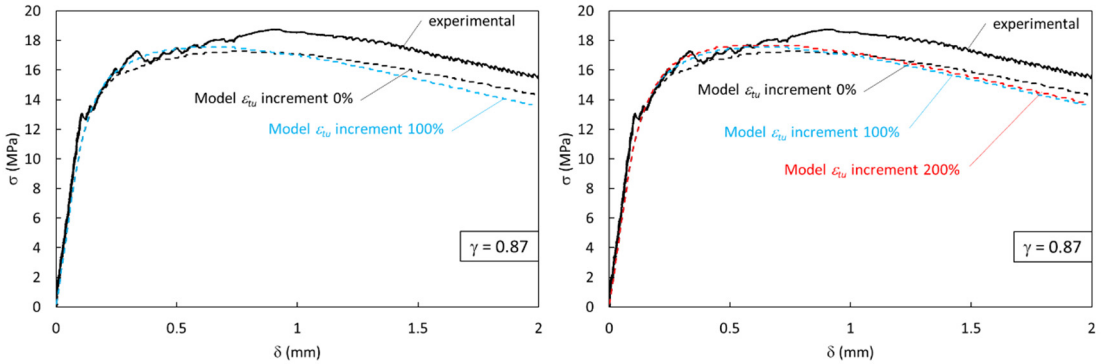

Figure 17 σ-δ response of the ε_{tu} variation in a strain-softening behavior specimen.

Table 4. Constitutive tensile parameters from applying 4P-IA and ε_{tu} variation

	constitutive tensile law					
	f_t (MPa)	f_{tu} (MPa)	ε_{tu} (‰)	E (MPa)	w_o (mm)	γ
4P-IA	8.08	7.03	3.35	54400	3.11	0.87
ε_{tu} 100% inc.	8.08	7.03	6.70	54400	3.11	0.87
ε_{tu} 200% inc.	8.08	7.03	10.05	54400	3.11	0.87

Parameter f_{tu}, which was obtained from applying 4P-IA, was calibrated using NLFEM as shown in Figure 16 for 64 specimens with different γ values; 32 specimens with 160 kg/m^3 and 32 with 130 kg/m^3. For each specimen, the increment in f_{tu}, denoted by variable *var*, required to fit the NLFEM σ-δ curve was obtained for the specimens with 130 kg/m^3 and 160 kg/m^3 of fibers for the different hardening coefficient (γ) values, as shown in Figure 18 (left). Therefore, a bilinear expression that relates the increment in the f_{tu} (*var*) percentage with the hardening coefficient (γ) can be deduced from Figure 18 (right).

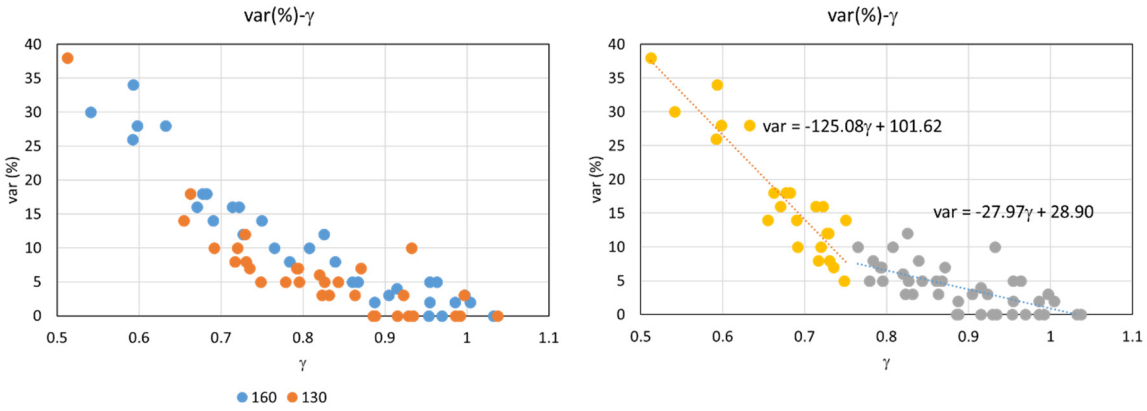

Figure 18 Relation var (%) - γ: 160 kg/m^3 and 130 kg/m^3 of fibers (left) and bilinear expression (right)

From Figure 18, Expression (4) can be deduced to relate the increment in the f_{tu} (*var*) percentage with the hardening coefficient (γ).

$$\begin{aligned} var &= 0 && \gamma \geq 1 \\ var &= -27.97 \cdot \gamma + 28.90 && 1 > \gamma > 0.75 \\ var &= -125.08 \cdot \gamma + 101.62 && 0.75 \geq \gamma \end{aligned} \tag{4}$$

Consequently for the UHPFRCs that exhibited SS ($\gamma < 1$) after applying 4P-IA, a correction of the f_{tu} parameter using Expression (5) can be made to fit the model response to the experimental one.

$$f_{tuc} = \left(1 + \frac{var}{100}\right) \cdot f_{tu} \tag{5}$$

Next the correction of f_{tu} (f_{tuc}) from Expression (5) was done for the same 65 specimens as in Figure 13, Figure 14 and Figure 15. The f_{tuc} parameter and the other constitutive parameters obtained from the simplified 4P-IA were implemented into NLFEM and compared to the experimental results. By considering the same previously defined criteria for CS (see Figure 12), the new relations between the hardening ratio (γ) and the CS at the four experimental deflection levels upon maximum experimental stress ($\delta_{\sigma maxexp}$): $0.25 \cdot \delta_{\sigma maxexp}$, $0.50 \cdot \delta_{\sigma maxexp}$, $\delta_{\sigma maxexp}$ and $1.25 \cdot \delta_{\sigma maxexp}$ for the 65 analyzed specimens including54 specimens of 160 kg/m^3 of fibers and 11 of 130 kg/m^3 (Figure 19).

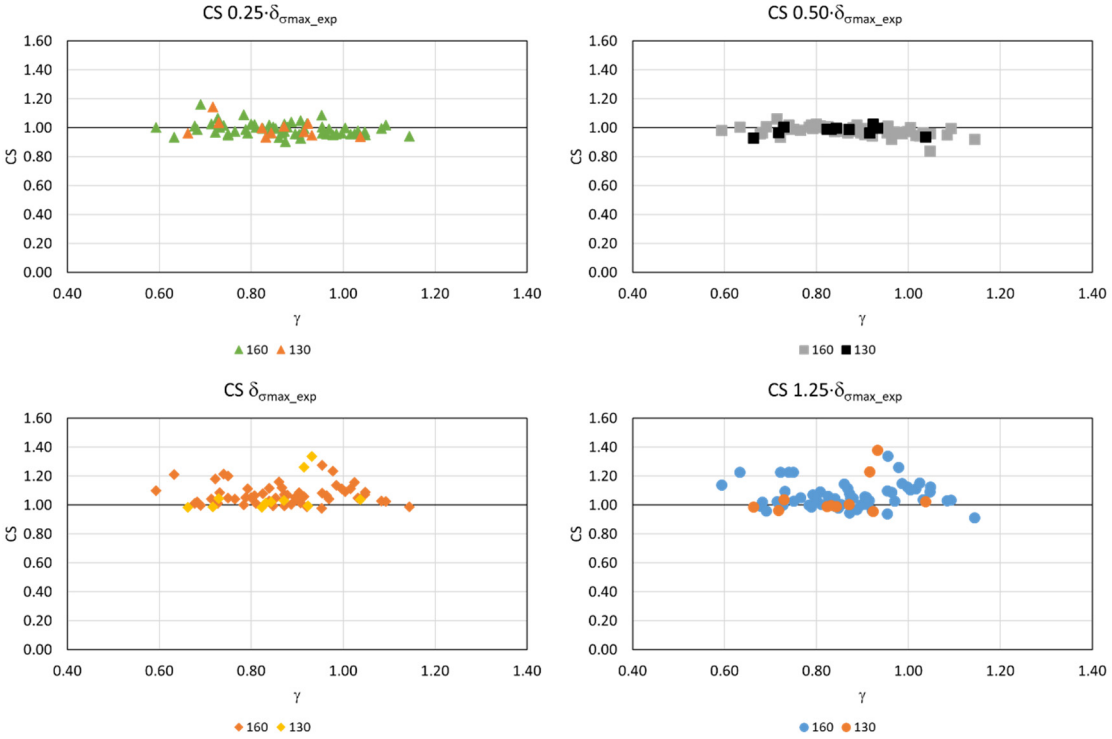

Figure 19. CS vs. γ at four δ levels when correcting f_{tu}

When comparing Figure 19 to Figure 13, the cloud of the CS-γ points in all the graphs are more aligned near 1.00 in Figure 19. In the early stages of the $\sigma - \delta$ curve, this took place at $0.25 \cdot \delta_{\sigma maxexp}$ and $0.50 \cdot \delta_{\sigma maxexp}$, Figure 19 shows very accurate results, which means that the model improved for SS, especially in $\gamma < 0.8$ in both cases. At the $\delta_{\sigma maxexp}$ and $1.25 \cdot \delta_{\sigma maxexp}$ levels, not only were the values more aligned, but the scatter of the results also reduced in the SS part ($\gamma < 1$). Therefore thanks to the f_{tu} correction, the results improved for SS and, consequently, the model became more accurate.

Figure 20 shows the relation between the energy calculated for the experimental ($A1_{exp}$) and numerical ($A1_{model}$) curves at the $\delta_{\sigma maxexp}$ level and the energy calculated for the experimental ($A2_{exp}$) and numerical ($A2_{model}$) curves at the $1.25 \cdot \delta_{\sigma maxexp}$ level for the same 65 specimens when making the f_{tu} correction in Expression (5).

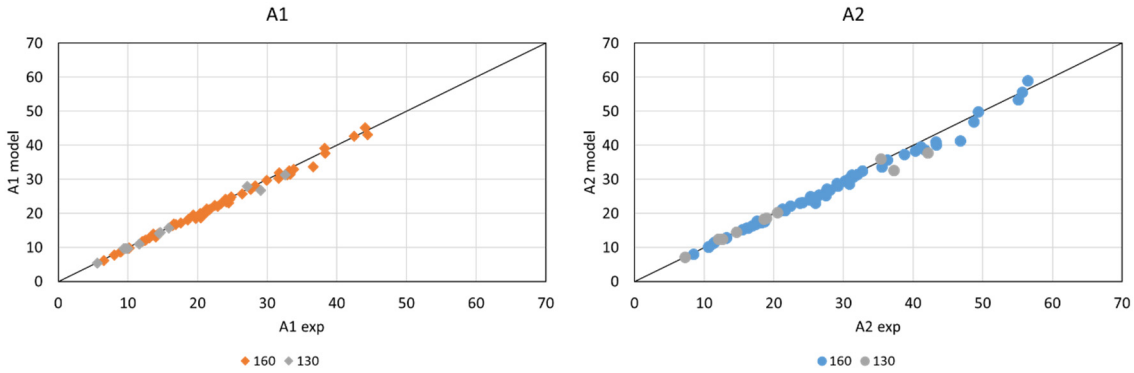

Figure 20. A1exp vs. A1model, A2exp vs. A2model when correcting f_{tu}

When comparing Figure 20 and Figure 14, the energy obtained in the experimental test came very close to that obtained in the model for the same specimen when the f_{tu} correction from Expression (5) was applied. The same trend was observed for the other specimens as the energy limited by $\delta_{\sigma maxexp}$ (A1) and that limited by $1.25 \cdot \delta_{\sigma maxexp}$ (A2). What this demonstrates is that the model which employed the f_{tu} correction for SS was more accurate and the obtained energy was similar to that obtained in the experimental test.

Figure 21 shows the relation between the experimental and numerical σ_{max} for the same 65 specimens when making the f_{tu} correction in Expression (5).

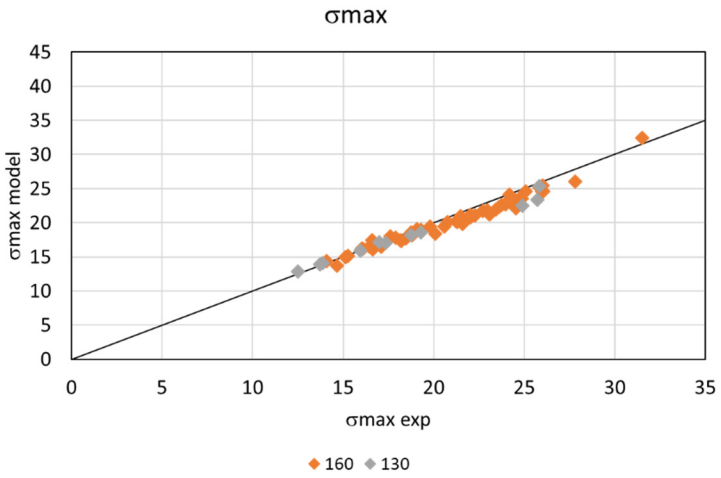

Figure 21. Experimental vs. model σ_{max} when correcting f_{tu}

When comparing Figure 21 and Figure 15, we see how, as in Figure 15, that the experimental σ_{max} value was higher than the numerical one for each specimen. Therefore, and as previously mentioned, this value demonstrated that the model was conservative in relation to the experimental results. According to Figure 21, the model more accurately fitted the experimental results when correcting the f_{tu} value following Expressions (4) and (5) for SS behavior (γ<1).

Therefore, as demonstrated above, the correction of the f_{tu} parameter for SS behavior (γ<1) using Expressions (4) and (5), and its application to NLFEM, led to an improved model response and made the prediction more accurate and reliable. Consequently, it could be stablished a standard method to characterize the UHPFRC tensile constitutive behavior covering all range from SH to SS following an easy to conduct experimental test and a simple and direct formulation.

5. Characteristic UHPFRC tensile constitutive behavior.

From the above-described work, it can be stated that anyone who proposes characterizing the tensile behavior of UHPFRC could do so no matter if it exhibited SH or SS. At this point, the characteristic σ-δ

curve of UHPFRC herein used was obtained to set the characteristic tensile parameters, which could be a reference for such concretes.

Of the 227 σ-δ curves, the characteristic σ-δ curve of the 158 specimens of 160 kg/m^3 and the 69 of 120-130 kg/m^3 of steel fiber were obtained. In Figure 22, the characteristic σ-δ curve for each amount of fibers is depicted.

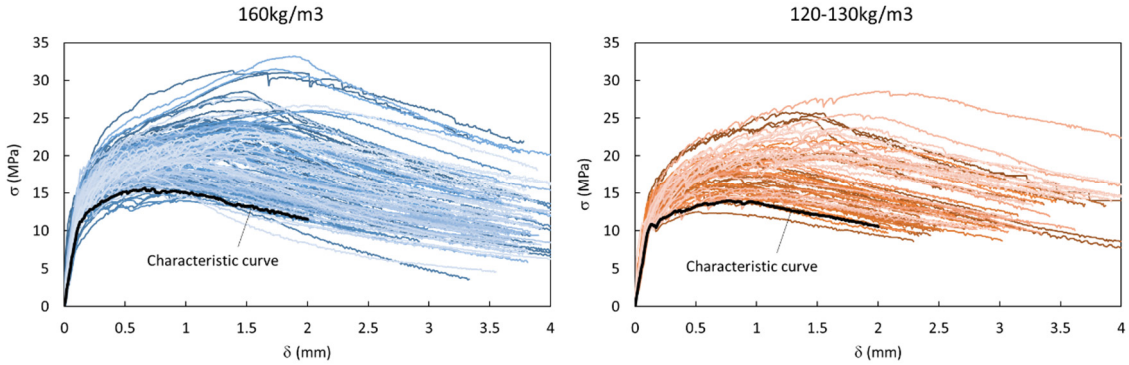

Figure 22 Characteristic σ-δ curve for the 160 kg/m^3 and 120-130 kg/m^3 steel fiber specimens

When the test ended, the equivalent flexural stress was obtained from the experimental load following (2). Using the σ-δ curve, 4P-IA was applied to obtain the tensile parameters (see Figure 2) following [10].

The values that defined the characteristic tensile parameters for the tensile behavior of UHPFRC with 120-130 kg/m^3 and 160 kg/m^3 of steel fibers were calculated and are shown in Table 5.

As seen in Table 5, the obtained characteristic tensile law for UHPFRC for both amounts of fibers exhibited SS, which was $\gamma < 1$. Therefore, it was necessary to correct the f_{tu} value following Expressions (4) and (5). The corrected tensile parameter f_{tuc} is detailed in Table 5. In this way, Table 5 provides details of the characteristic tensile constitutive parameters for UHPFRC with 120-130 kg/m^3 and 160 kg/m^3 of steel fibers. In Figure 23, the comparison made between the characteristic experimental σ-δ curve and the NLFEM σ-δ curve, when the characteristic tensile parameters from Table 5 were used in the model, is depicted for the UHPFRC with both amounts of fibers. Hence, the comparison in Figure 23 demonstrates the employed method's reliability to obtain the constitutive tensile parameters of UHPFRC in Table 5.

Table 5 Characteristic constitutive tensile parameters for 120-130 and 160 kg/m^3 of fiber UHPFRC

Steel fibers (kg/m^3)	UHPFRC characteristic constitutive tensile law						
	f_t (MPa)	f_{tu} (MPa)	γ	f_{tuc} (MPa)	ε_{tu} (‰)	E (MPa)	w_o (mm)
120-130	6.51	5.12	0.79	5.47	2.62	42500	2.65
160	7.03	6.32	0.90	6.56	1.71	46750	2.35

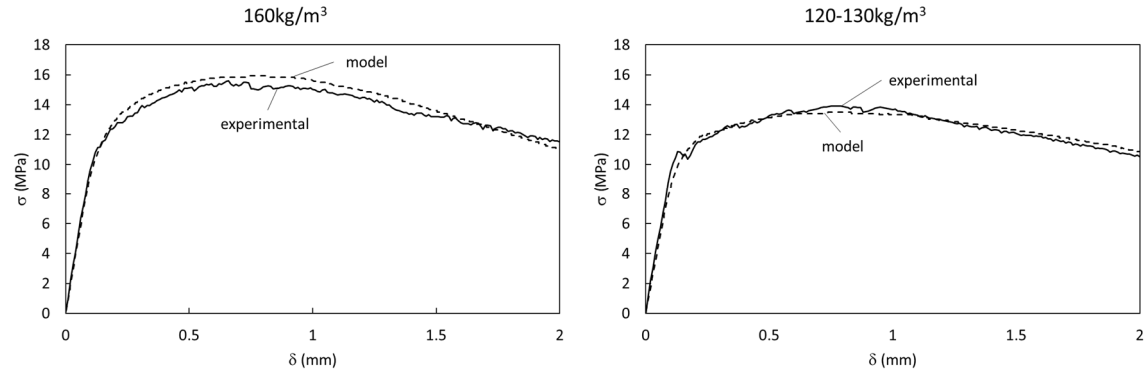

Figure 23 Characteristic σ-d curves: FEM using corrected tensile parameters vs. experimental response

6. Predicting application to obtain UHPFRC tensile constitutive behavior

By bearing in mind the huge experimental database that we present here, namely 227 UHPFRC 4PBT specimens, a predicting application was developed to avoid variability in the application of a simplified inverse analysis. With this application, it was possible to obtain the constitutive tensile parameters of UHPFRC by introducing only the σ-δ curve obtained from 4PBT without having to apply 4P-IA and the correction for SS because this was already considered in the predicting application.

The objective was, by obtaining the experimental σ-δ from 4PBT as input and the tensile constitutive parameters as output, to generate an application which, by introducing the experimental σ-δ curve, directly returned the tensile constitutive parameters. With this application, it was possible to avoid the variability due to the interpretation and application of the simplified 4P-IA because the whole database was produced in the same way. In this sense, the variability in the final result could be restricted to other effects more related to the casting process, pouring system and preservation of the specimens, and the suitability of the testing method used to characterize the tensile behavior of UHPFRC (in this case, the 4PBT).

The application was developed using a kriging predictor adaptation from the DACE (Design and Analysis of Computer Experiments) software package. This is a Matlab toolbox developed by [34] to work with kriging approximations with computer models. In this application, the addressed computer models were deterministic.

The required inputs to build the model were:

- S: a matrix containing all the σ-δ experimental curves. Each column of the matrix was a σ-δ curve. In this case, 200 curves were used. That is, the model "learned" by using these curves as a database. Therefore, the matrix would contain 200 columns. The number of rows was the number of points of the σ-δ curve
- Y: a matrix containing the responses of each curve (column) of S. These were the tensile constitutive parameters: f_t, f_{tuc} (f_{tu} corrected by the softening function using Expressions (4) and (5)), ε_{tu}, E and w_o. Each column of the matrix corresponded to each parameter, and the number of rows was determined by the number of used curves, which was 200 in this case. Each row of matrix Y was the response of each column of matrix S
- The regression model used here was a zero-order polynomial
- The correlation model used here was the exponential one

The model was built using this information. This can be considered the information which the model "learned" with and, accordingly, it would be able to predict.

To calibrate the model, 27 specimens were used. Therefore, the 27 experimental σ-δ curves were introduced into the model using a matrix with 27 columns (one column for each curve). With these, the model predicted the tensile constitutive parameters for each curve. Figure 24 depicts a comparison made between the prediction response and the result if 4P-IA was applied (the "real" response) for the 27 evaluated specimens.

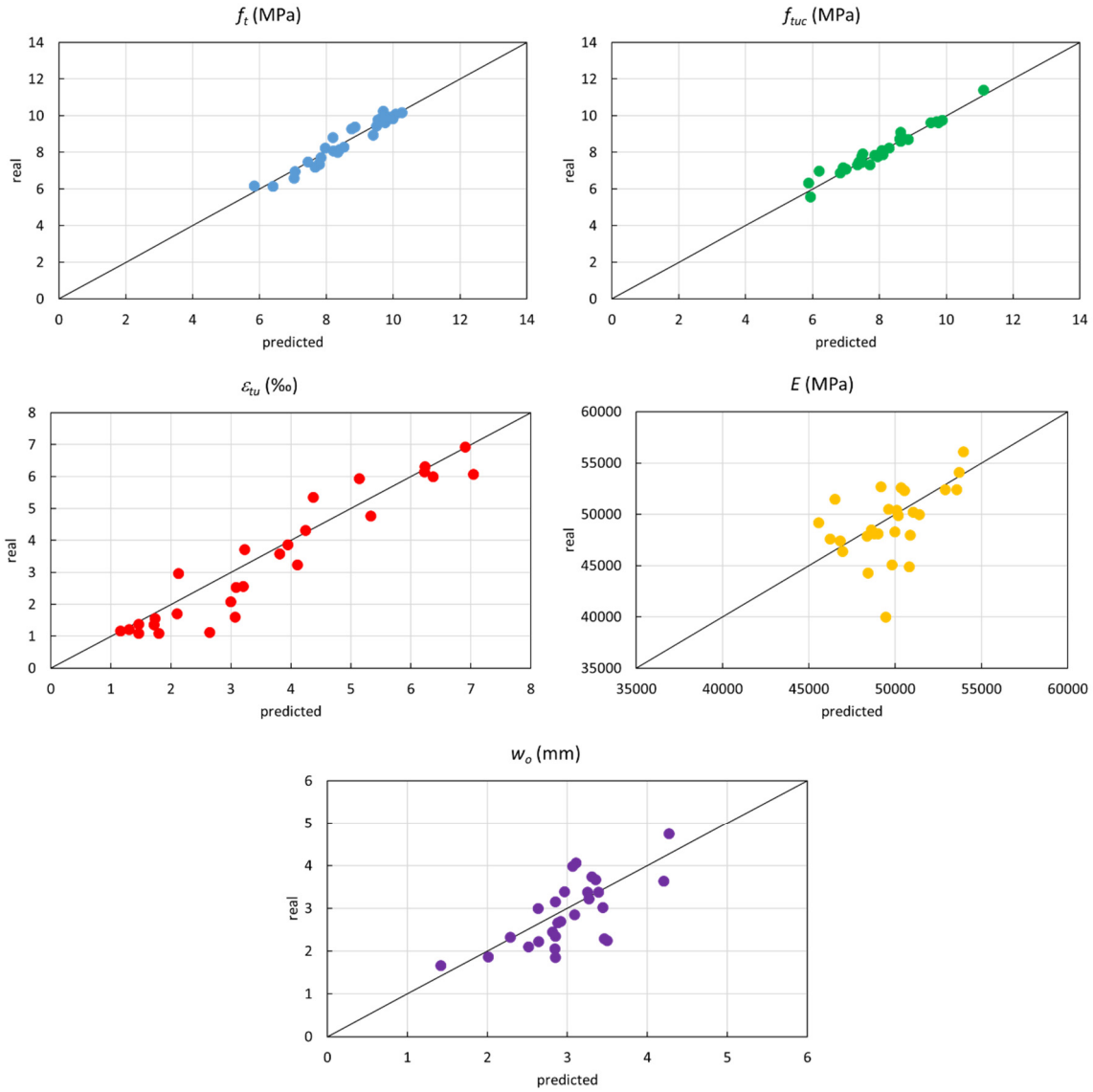

Figure 24 UHPFRC Tensile constitutive parameters: predicted values vs. real values

As observed in Figure 24, the predicted f_t and f_{tuc} values were very accurate. The ε_{tu} and w_o values were reliable and, even though the E values seemed to show some point with slight deviation, it could be generally considered a good prediction.

Moreover, a prediction was made of the characteristic constitutive tensile parameters from the 4PBT curves depicted in Figure 22 (see Table 6). When the values predicted in Table 6 were compared to those in Table 5, the prediction was quite good.

Table 6 The predicted characteristic constitutive tensile parameters for 120-130 and 160 kg/m³ of fiber UHPFRC

Steel fibers (kg/m3)	UHPFRC predicted characteristic constitutive tensile law				
	f_t (MPa)	f_{tuc} (MPa)	ε_{tu} (‰)	E (MPa)	w_o (mm)
120-130	6.18	5.74	2.63	46296	3.07
160	6.78	6.60	2.00	45974	2.25

Therefore by using 200 UHPFRC 4PBT specimens (139 with 160 kg/m^3 of steel fibers and 61 with 120-130 kg/m^3), a prediction model was developed that was able to make an accurate prediction of the UHPFRC tensile constitutive parameters, f_t, f_{tuc}, ε_{tu}, E and w_o, from the 4PBT experimental σ-δ curve. This application

is simple, direct and avoids variability in the simplified 4P-IA due to the interpretation and application of the inverse analysis. This application can become a good starting point in this direction.

7. Concluding remarks

This work intended to take a step forward in the tensile characterization of UHPFRC in both SH and SS. As most processes have been conceived to characterize SH UHPFRC, in this work a justification of using SS UHPFRC was made. As a result, a simple process to obtain tensile behavior was set up. Therefore, the following conclusions are outlined.

There is a need to establish a complete process to characterize UHPFRC tensile behavior in either SH or in SS behavior. This process starts with the experimental test which, in this work, was the 4PBT given its simplicity.

To move from the experimental σ-δ response in bending to tensile behavior, a simplified four point inverse analysis (4P-IA), developed by the research group, was used. As it was developed for the UHPFRC exhibiting the SH tensile response, its application to UHPFRC with SS needed to be adapted. Consequently, an experimental program of 227 4PBT that went from the SH behavior to the SS behavior was run using UHPFRC with 120-130 kg/m^3 and 160 kg/m^3 of steel fibers. As demonstrated, 4P-IA worked well for UHPFRC with SH, but was still too conservative for SS. Therefore, a parametrical study that focused on the ε_{tu} and f_{tu} parameters was performed to study their influence on the σ-δ response using NLFEM. The f_{tu} parameter had a direct influence on the model's response and 4P-IA underestimated the f_{tu} value, which led to a conservative result. However, the influence of the variation in ε_{tu} was considered negligible.

A correction of 4P-IA for SS UHPFRC was made in f_{tu} terms after analyzing 65 specimens from the experimental program with different strain-hardening ratio (γ) values, and after the calibration of f_{tu} from 64 specimens from the experimental program. This correction led to a more accurate response in stress and energy terms at different levels. Consequently, UHPFRC was characterized in tensile behavior terms by following a reliable process.

Having set up a reliable method to characterize UHPFRC tensile behavior, the characteristic σ-δ curve of UHPFRC from the experimental data was extracted. Therefore, the characteristic tensile behavior parameters could be obtained for UHPFRC with 120-130 kg and 160 kg/m^3 of steel fibers. These values could act as a reference for UHPFRC with these amounts of fibers.

Using the extensive experimental program herein employed, a predictive application for predicting the tensile UHPFRC parameters from the σ-δ curve from 4PBT was developed. The prediction gave reliable results. The application is simple, direct and avoids not only variability in the simplified 4P-IA due to misinterpretations, but also applying the inverse analysis.

Acknowledgements

This work forms part of Project "BIA2016-78460-C3-1-R" supported by the State Research Agency of Spain and the European Union's Horizon 2020 ReSHEALience Project (Grant Agreement No. 760824)

References

[1] D.-Y. Yoo, W. Shin, B. Chun, Corrosion effect on tensile behavior of ultra-high-performance concrete reinforced with straight steel fibers, Cem. Concr. Compos. 109 (2020) 103566. https://doi.org/https://doi.org/10.1016/j.cemconcomp.2020.103566.

[2] Q. Song, R. Yu, Z. Shui, S. Rao, X. Wang, M. Sun, C. Jiang, Steel fibre content and interconnection induced electrochemical corrosion of Ultra-High Performance Fibre Reinforced Concrete (UHPFRC), Cem. Concr. Compos. 94 (2018) 191–200. https://doi.org/https://doi.org/10.1016/j.cemconcomp.2018.09.010.

[3] E. Fehling, M. Schmidt, J. Walraven, T. Leutbecher, S. Fröhlich, Ultra-high performance concrete UHPC: Fundamentals, design, examples, John Wiley & Sons, 2014.

[4] D.-Y. Yoo, N. Banthia, Mechanical properties of ultra-high-performance fiber-reinforced

concrete: A review, Cem. Concr. Compos. 73 (2016) 267–280.

[5] G.J. Parra-Montesinos, H.W. Reinhardt, A.E. Naaman, High Performance Fiber Reinforced Cement Composites 6 HPFRCC 6, (n.d.).

[6] H.W. Reinhardt, G.J. Parra-Montesinos, H. Garrecht, HPFRCC-7: Proceedings of the 7th RILEM Workshop on High Performance Fiber Reinforced Cement Composites, Fraunhofer IRB Verlag, 2015.

[7] H. Yokota, K. Rokugo, N. Sakata, (JSCE-2008) Recommendations for Design and Construction of High Performance Fiber Reinforced Cement Composites with Multiple Fine Cracks (HPFRCC), (2008). https://doi.org/http://dx.doi.org/10.1016/j.dci.2010.01.003.

[8] A.M.T. Hassan, S.W. Jones, G.H. Mahmud, Experimental test methods to determine the uniaxial tensile and compressive behaviour of ultra high performance fibre reinforced concrete (UHPFRC), Constr. Build. Mater. 37 (2012) 874–882. https://doi.org/10.1016/j.conbuildmat.2012.04.030.

[9] A. Mallat, A. Alliche, A modified tensile test to study the behaviour of cementitious materials, Strain. 47 (2011) 499–504.

[10] J.Á. López, Characterisation of the tensile behaviour of UHPFRC by means of four-point bending tests, PhD Thesis, Univ. Politècnica València, València. (2017). https://doi.org/10.4995/Thesis/10251/79740.

[11] F. Baby, B. Graybeal, P. Marchand, F. Toutlemonde, UHPFRC tensile behavior characterization: Inverse analysis of four-point bending test results, Mater. Struct. Constr. 46 (2013) 1337–1354. https://doi.org/10.1617/s11527-012-9977-0.

[12] S. Qian, V.C. Li, Simplified Inverse Method for Determining the Tensile Strain Capacity of Strain Hardening Cementitious Composites, J. Adv. Concr. Technol. 5 (2007) 235–246. https://doi.org/10.3151/jact.5.235.

[13] T. Kanakubo, Tensile Characteristics Evaluation Method for Ductile Fiber-Reinforced Cementitious Composites, J. Adv. Concr. Technol. 4 (2006) 3–17. https://doi.org/10.3151/jact.4.3.

[14] C. Soranakom, B. Mobasher, Closed-form moment-curvature expressions for homogenized fiber-reinforced concrete, ACI Mater. J. 104 (2007) 351–359. https://doi.org/10.14359/18824.

[15] F. Baby, B. Graybeal, P. Marchand, F. Toutlemonde, Proposed flexural test method and associated inverse analysis for ultra-high-performance fiber-reinforced concrete, ACI Mater. J. 109 (2012) 545–555. https://doi.org/10.14359/51684086.

[16] M. Maalej, V.C. Li, Flexural Strength of Fiber Cementitious Composites, ASCE J. Mater. Civ. Eng. 6 (1994) 390–406. https://doi.org/10.1061/(ASCE)0899-1561(1994)6:3(390).

[17] S. Rigaud, G. Chanvillard, J. Chen, Characterization of Bending and Tensile Behavior of Ultra-High Performance Concrete Containing Glass Fibers, in: G.J. Parra-Montesinos, H.W. Reinhardt, A.E. Naaman (Eds.), High Perform. Fiber Reinf. Cem. Compos. 6 HPFRCC 6, Springer Netherlands, Dordrecht, 2012: pp. 373–380. https://doi.org/10.1007/978-94-007-2436-5_45.

[18] K. Gröger, Johannes, Viet tue, Nguyen, Wille, Bending Behaviour and Variation of Flexural Parameters of UHPFRC, in: 3rd Int. Symp. UHPC Nanotechnol. High Perform. Constr. Mater., kassel university press GmbH, 2012: pp. 419–426.

[19] L. Ostergaard, R. Walter, J.F. Olesen, Method for determination of tensile properties of engineered cementitious composites (ECC), in: Constr. Mater. Proc. ConMat'05 Mindess Symp., 2005: p. 74.

[20] J.Á. López, P. Serna, J. Navarro-Gregori, E. Camacho, An inverse analysis method based on deflection to curvature transformation to determine the tensile properties of UHPFRC, Mater. Struct. 48 (2015) 3703–3718. https://doi.org/10.1617/s11527-014-0434-0.

[21] J.L. Tailhan, P. Rossi, E. Parant, Inverse numerical approach to determine the uniaxial tensile behaviour of a stress hardening cement composite from its bending behaviour, in: Fiber Reinf.

Concr. 2004, Proc. 6th Int. RILEM Symp. M. Di Prisco, R. Felicetti, GA Plizzari, Eds, 2004: pp. 913–922.

[22] Swiss Society of Engineers and Architects SIA, Sia 2052, (2016) 48.

[23] S. AFGC, Bétons fibrés à ultra-hautes performances–Recommandations, AFGC, Fr. (2013).

[24] J.A. López, P. Serna, J. Navarro-Gregori, Advances in the development of the first UHPFRC Recommendations in Spain: Material classification, design and characterization, in: F. Toutlemonde & J. ResplendinoT.Ch. (Ed.), UHPFRC 2017 Des. Build. with UHPFRC New Large-Scale Implementations, Recent Tech. Adv. Exp. Stand., RILEM Publications SARL, 2017: pp. 565–574.

[25] J.Á. López, P. Serna, J. Navarro-Gregori, H. Coll, A simplified five-point inverse analysis method to determine the tensile properties of UHPFRC from unnotched four-point bending tests, Compos. Part B Eng. 91 (2016) 189–204. https://doi.org/10.1016/j.compositesb.2016.01.026.

[26] N. Gowripalan, R.I. Gilbert, Design guidelines for ductal prestressed concrete beams, Ref. Artical, Univ. NSW. (2000).

[27] Japan Society of Civil Engineers, Recomendations for Design and Construction of High Performance Fiber Reinforced Composites with Multiple Fine Cracks (HPFRCC), Concr. Eng. Ser. 82. (2008).

[28] H.G. Russell, B.A. Graybeal, H.G. Russell, Ultra-high performance concrete: A state-of-the-art report for the bridge community., United States. Federal Highway Administration. Office of Infrastructure …, 2013.

[29] Association Francaise de Normalisation, Concrete-Ultra-high performance fibre-reinforced concrete-specifications, performance, production and conformity, NFP 18 470 2016. (2016).

[30] Association Francaise de Normalisation, National addition to Eurocode 2- Design of concrete structures: specific rules for ultra-high performance fibre-reinforced concrete (UHPFRC), NFP 18 710 2016. (2016).

[31] E.J. Mezquida-Alcaraz, J. Navarro-Gregori, J. Angel Lopez, P. Serna-Ros, Validation of a non-linear hinge model for tensile behavior of UHPFRC using a Finite Element Model, Comput. Concr. 23 (2019) 11–23.

[32] E.J. Mezquida-Alcaraz, J. Navarro-Gregori, J.A. López, P. Serna-Ros, Numerical Validation of a Simplified Inverse Analysis Method to Characterise the Tensile Behaviour of UHPFRC, in: FRC2018 Fibre Reinf. Concr. from Des. to Struct. Appl. Jt. ACI-Fib-RILEM Int. Work., 2018.

[33] DIANA (Software), User's Manual -- Release 10.2, TNO DIANA, Netherlands. (2017). https://dianafea.com/manuals/d102/Diana.html.

[34] S.N.L. and J.S. H. B. Nielsen, DACE - A Matlab Kriging Toolbox, Informatics Math. Model. Tech. Univ. Denmark, DTU. (2002). http://localhost/pubdb/p.php?1460.